Influence of steric effects on the emission behavior of pyrene-based blue luminogens

Zhixin Xie[a], *Wei Liu*[a], *Yiwei Liu*[a], *Xinyi Song*[a], *Heng Zheng,*[a] *Xiang Su*[a]*, *Carl Redshaw*[b], *Xing Feng*[a]*

[a] Guangdong University of Technology, Guangzhou 510006, P. R. China

[b] Chemistry, School of Natural Sciences, University of Hull, Hull, Yorkshire HU6 7RX, UK.

ABSTRACT: Pyrene-based derivatives have been widely deployed in organic luminescent materials, because of their bright fluorescence, high charge-carrier mobility and facile modification. Nevertheless, the fluorescence output of conventional pyrenes is prone to quenching upon aggregation due to extensive intermolecular π–π stacking interactions. To address this issue, a set of new *Y*-shaped pyrene-containing luminogens have been synthesized from a new bromopyrene chemical precursor, 2-hydroxyl-7-*tert*-butyl-1,3-bromopyrene, where the bromo and hydroxyl groups at the pyrene core can be readily modified to obtain the target products and provide great flexibility in tuning the photophysical performances. When the hydroxy group at the 2-position of pyrene was replaced by a benzyl group, the steric hindrance of the benzyl group not only efficiently inhibits the detrimental intermolecular π–π stacking interactions, but also rigidifies the molecular conformation, which results in a narrow-band blue emission. Moreover, the TPE-containing compounds **2c** and **3c** possessed characteristic aggregation-induced emission (AIE) properties with fluorescence quantum yields of up to 66% and 38% in the solid state, respectively. Thus, this article has methodically investigated the factors influencing the optical behavior of XXX, such as intermolecular interactions, and the steric effects of the substituent group, thereby opening up the potential to develop narrow-band pyrene-based blue emitters for OLED devices applications.

KEYWORDS: Pyrene, blue emitter, aggregation-induced emission, steric effect

1. Introduction

Polycyclic aromatic hydrocarbons (PAHs) featuring large π-conjugated architectures are a significant category of functional materials by virtue of their remarkable photophysical, electrical and mechanical performances[1-3] and have been successfully applied in diverse fields, ranging from organic field-effect transistors,[4,5] organic photovoltaic cells,[6-9] organic/quantum dot light-emitting diodes[10-12] to fluorescence sensors.[13-15] As one of the extensively used and representative families of PAHs, pyrenes are chemically stable and contain four integrated benzene rings with extended π-electron delocalization.[16] The unique flat aromatic scaffold endows pyrenes with salient properties, such as deep blue fluorescence, high charge-carrier mobility and prominent hole injection capacity, making them excellent candidates for organic optoelectronic materials, chemosensors, and bioimaging applications.[17-20] However, the fluorescence output of pyrene aggregates are usually inferior to what can be achieved in their respective solutions, and this hampers their potential high-technological application in fluorescence-relevant areas.[21,22] The weakened emission in the aggregated state may be attributed to the facile generation of detrimental substances such as excimers, given that the planar structure of pyrene tends to undergo intense intermolecular π–π stacking interactions once aggregated. Therefore, exploring feasible approaches to promote the aggregate-state fluorescence of pyrenes is of great interest when trying to facilitate their latent applications in organic optoelectronics and other extensive scenarios.

To address this issue, researchers have recently developed several strategies to new pyrene-based emitters with high-performance emission features. One of the main strategies is to employ bulky groups such as a *tert*-butyl substituent to enhance the steric hindrance present, which results in reduced excimer formation and/or π–π stacking interactions in the aggregated state.[23-25] Another prospective strategy has focused on developing aggregation-induced emission luminogens (AIEgens) to inhibit the fluorescence suppression of conventional pyrene emitters upon aggregation.[26-29] Generally, pyrene-based emitters with AIE properties exhibit weak emission in dilute solution, but could boost the fluorescence brightness in the aggregated state, which eventually has helped to solve the above-mentioned fluorescence quenching issue.[17,22] In the light of the generally acknowledged working mechanism of AIE, the basic design principle of AIEgens lies in the distorted architectures and twisted molecular rotors. Such a design can lead to the efficient constraint of the intermolecular π–π stacking interactions and a resulting high fluorescence quantum yield (QY) in the aggregated state.[30-32] Thus, pyrene-based AIEgens have been explored successfully through functionalization of pyrene at certain sites to access high-performance luminescent materials.

On the other hand, organic blue emitters as one of the significant components for full-color displays also have certain drawbacks due to the limited stability and relatively large energy gaps, etc.[33,34] It still remains a challenge to construct high-performance blue emissive pyrene-based AIEgens through molecular engineering. Pyrene as a great building block for blue fluorescent materials has become a focus of much research given that it possesses, not only the intrinsic blue-light emission, but also is readily functionalized at different active sites depending on the controllable experimental condition,[35-38] and this can result in diverse photophysical and chemical properties. Among them bromo-containing pyrene-based chemical intermediates can act as pivotal precursors for the synthesis of assorted C-functionalized pyrene-based luminescent materials *via* metal-catalyzed cross-coupling reactions.[39-41] Thus, developing novel bromo-containing pyrene-based precursors is of great significance, and can open up infinite possibilities in the field of new pyrene-containing multifunctional optoelectronic materials for real applications. Up to now, a limited number of meaningful bromo-containing pyrene-based precursors have been successfully exploited.[42,43]

Recently, our group developed a new pyrene-based chemical intermediate, namely 2-hydroxyl-7-*tert*-butyl-1,3-bromopyrene (**1**), which was further involved in a metal-catalyzed coupling reaction to construct a narrow-band pyrene-based blue emitter with FWHM less than 20 nm in the solid state. However, the reported compounds display a relative low fluorescence quantum yield (less than 0.1), the main reason for which is ascribed to the presence of the hydroxyl group, which results in strong intermolecular interactions. Thus, the key issue is to endow the pyrene-based emitters with blue emission, high fluorescence quantum yield and narrow-band emission for fabricating blue OLED devices with high color purity.

Considering the above issues and based on previous work on pyrene-based luminescence in our group, we employed intermediate **1** as a precursor, and a new set of *Y*-shaped luminescent materials were synthesized via a Suzuki–Miyaura coupling reaction. Bulky groups (such as triphenylamine (TPA) and tetraphenylethylene (TPE)) were introduced at the 1,3-positions of the pyrene core, and this played a vital role in efficiently preventing the detrimental intermolecular π–π stacking interactions, leading to high-efficiency emission in the solid state. According to our previous reports,[41] the methylation of the -OH at position 2 of pyrene can improve the fluorescence quantum yield in the solid state. Furthermore, in this work, the hydroxy group at the 2-position was replaced by a bulky 4-(trifluoromethyl)benzyl group, which not only acted as the large steric group but also tuned the photophysical properties via regulating the intermolecular hydrogen-bond interactions.[41] Finally, the target compounds exhibited a blue-shifted emission and a narrower FWHM, as well as a boosted fluorescence quantum yield in the solid state (Scheme 1).

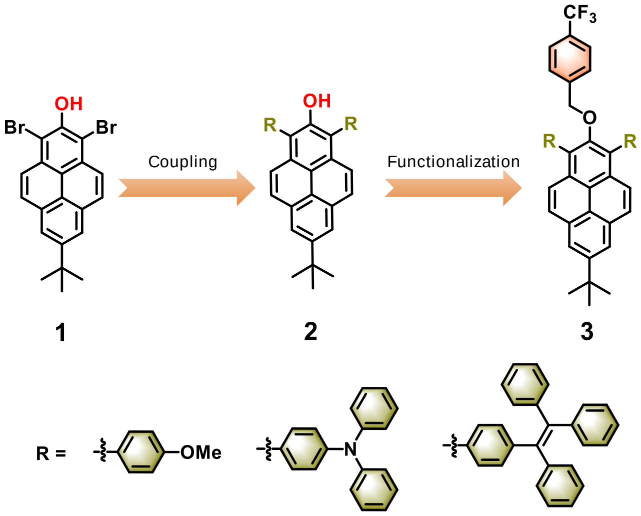

Scheme 1. Schematic diagram of the molecular strategy.

3. Results and discussion

3.1 Synthesis and Characterization

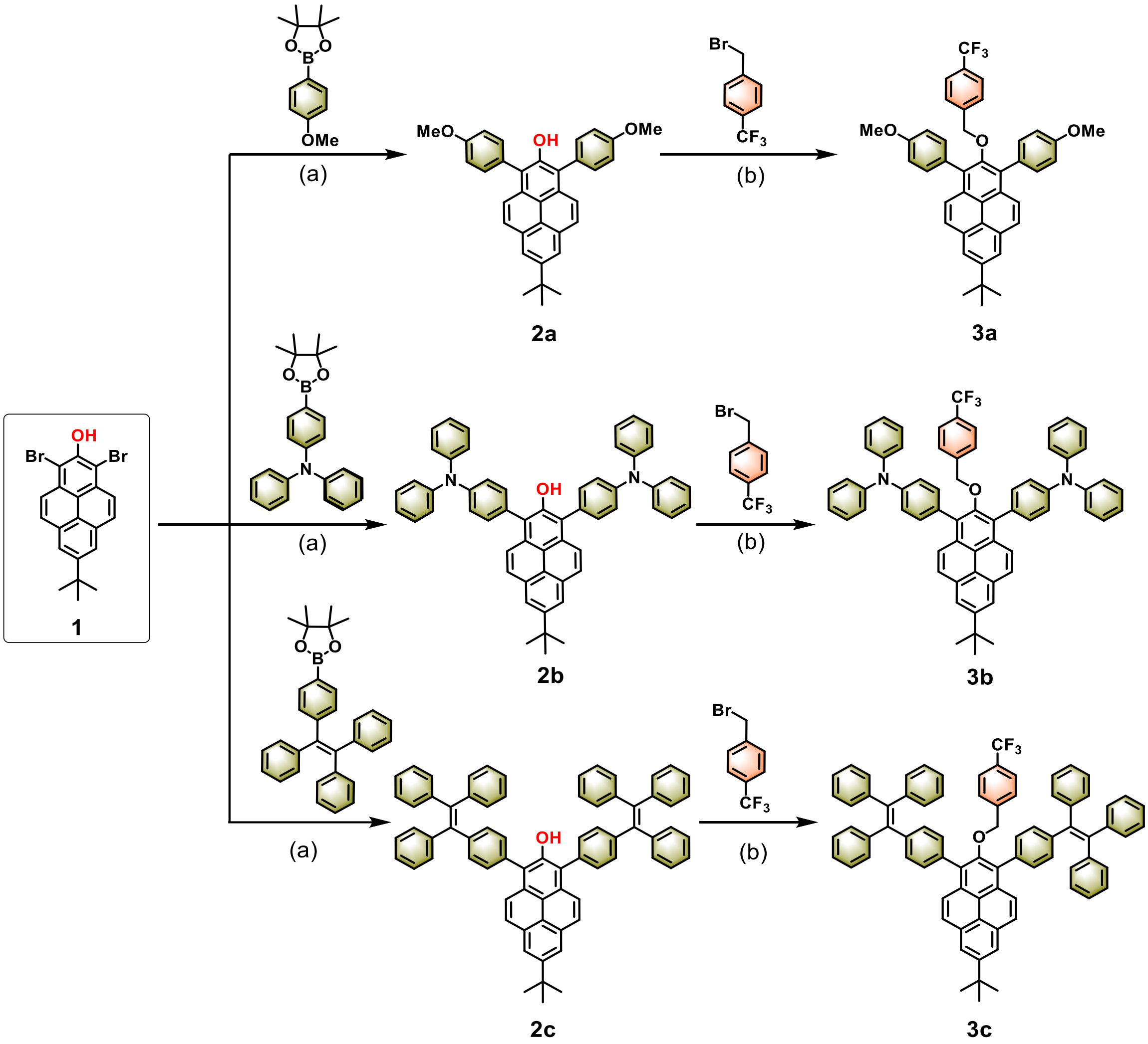

Scheme 2. Synthetic routes of **2** and **3**. (a) Pd(PPh$_3$)$_4$, K$_2$CO$_3$, toluene/ethanol/H$_2$O, 90 °C, 24 h; (b) Cs$_2$CO$_3$, extra dry DMF.

To more fully understand the effect of the substituent groups at the 1,3-positions and 2-position on the optical properties of pyrene, we prepared the families of luminescent compounds **2** and **3** using pyrene as the core skeleton with different substitutions located at the 1,3-positions and 2-position, respectively. According to the synthetic routes in Scheme 2, firstly, the key intermediate 2-hydroxyl-7-*tert*-butyl-1,3-bromopyrene **1** was synthesized via the bromination reaction of 7-*tert*-butyl-2-hydroxypyrene with *N*-bromosuccinimide (NBS) in 57% isolated yield. Subsequently, triphenylamine (TPA) or tetraphenylethylene (TPE) units were introduced at the 1,3-positions via a Pd-catalyzed Suzuki−Miyaura coupling reaction between the bromo-substituted intermediate **1** and the corresponding arylboronic acid ester to afford the target 1,3-disubstituted pyrene derivatives **2a-2c** in good yield. In order to further regulate the steric effect and the optical behavior, the hydroxyl group was modified with 1-(bromomethyl)-4-(trifluoromethyl)benzene through a Williamson reaction to afford the compounds **3** with a large steric unit located at the 2-position. The target compounds were characterized by ^1H and $^{13}C\{^1H\}$ NMR spectroscopy (Figures S1-S13) and high-resolution mass spectrometry (HRMS, Figures S14-S19). They possessed good solubility in common organic solvents, such as dichloromethane (DCM), tetrahydrofuran (THF), chloroform ($CHCl_3$), acetone, etc., which is convenient for the subsequent studies of their photophysical properties and is also conducive to their future practical applications.

3.2 Thermal stability analysis

Thermal stability analysis can evaluate heat resistance and the retention ability of material properties at high temperatures. The thermal stability is related to chemical structure, degree of π-conjugation, molecular weight, etc. Excellent thermal stability is a perquisite for a compound to be utilized in the manufacture of optoelectronic devices such as OLEDs and other functional applications.[44,45] Thus, the thermal stability properties of **2** and **3** were explored by thermalgravimetric analysis (TGA) under N_2 atmosphere with a heating rate of 10 °C/min. As presented in Figure 1, the decomposition temperatures (T_d, corresponding to 5% weight loss) of compounds **2** with a hydroxyl group are higher compared with the corresponding compounds **3** containing a 4-(trifluoromethyl) benzyl moiety at the 2-position. For example, compounds **2** showed high thermal stability over the range of 364-495 °C, indicating that the presence of intermolecular hydrogen bonds in compounds **2** can enhance the thermal stability. However, when the hydroxyl group was replaced with a 4-(trifluoromethyl) benzyl moiety, the T_d of **3a-3c** decreased to 327 °C for **3a**, 331 °C for **3b** and 369 °C for **3c**, respectively. According to the TGA data, when the temperature was raised to around 320 °C, a sharp decrease in weight occurred for **3a**-**3c** with a weight loss of about 23%, 15% and 16% respectively, which may be attributed to the removal of 4-(trifluoromethyl) benzyl moiety with cleavage of the C-O bond. Additionally, the larger π-conjugated structure is also contributing to elevating the thermal decomposition temperatures, as observed for the higher T_d of TPE-containing compounds (**2c** and **3c**) relative to the corresponding *p*-methoxyphenyl- and TPA-substituted compounds (**2a**,

2b and **3a**, **3b**). Moreover, as the temperature was raised to about 800 ºC, the compounds **2a**, **2b**, **2c**, **3a**, **3b** and **3c** still possessed a carbonization residue (char yield) of 10%, 12%, 38%, 36%, 40% and 36%, respectively. All the above results identified the remarkable thermal stability of the desired compounds.

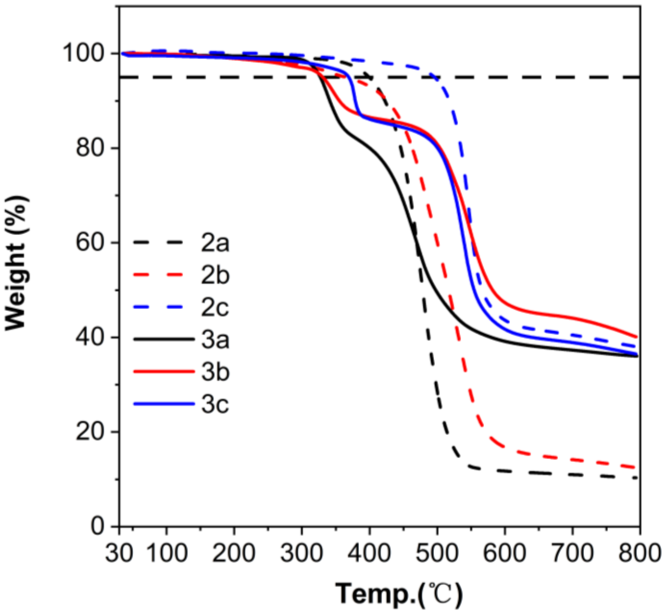

Figure 1. Thermalgravimetric analysis of **2** and **3**.

3.3 Single Crystal X-ray Diffraction Analysis.

Single crystals of the compound **3a** were cultivated via slow evaporation of a hexane/dichloromethane solution, and were further characterized by X-ray crystallographic analysis. The compound **3a** crystallizes in the monoclinic system with the P $_{21/n}$ space group, and an asymmetric unit containing four molecules (Table S1). As shown in Figure 2, the twist angles between the phenyl rings (at the 1,3-positions of pyrene) and the pyrene ring are 63.3 (3)^{o} and 53.0 (3)^{o}, respectively. While the 4-(trifluoromethyl)benzyl moiety adopts a face-to-face π-π stacking pattern with the phenyl rings at an average distance of 3.975 Å, which was further fixed by the C-H···π (C38-H38···C12: 2.996 Å, C37-H37···C14: 3.255 Å, C35-H35···C10: 2.909 Å and C40-H40···C2: 3.045 Å) interactions and C18-H18···F2 (2.757 Å) interactions along the *b*-axis. The distance of the centroid-to-centroid between two phenyl ring is 3.975 Å, thus, the calculated aligned angle value is 59.7^{o}, which is larger than 54.7^{o}. According to the McRaés theory, it is regarded as an H-aggregate.[46] On the other hand, no clear π-π stacking interactions were observed between the pyrene core, and adjacent molecules were connected by C1-H1···O2 (2.659 Å) and C4-H4···F1 (2.671 Å) interactions along *c*-axis, respectively. Thus, the presence of several weak intermolecular interactions plays a significant role to restrict the molecular motion, resulting in a rigid molecular backbone, which facilitates a narrower emission for the target compounds in the solid state.

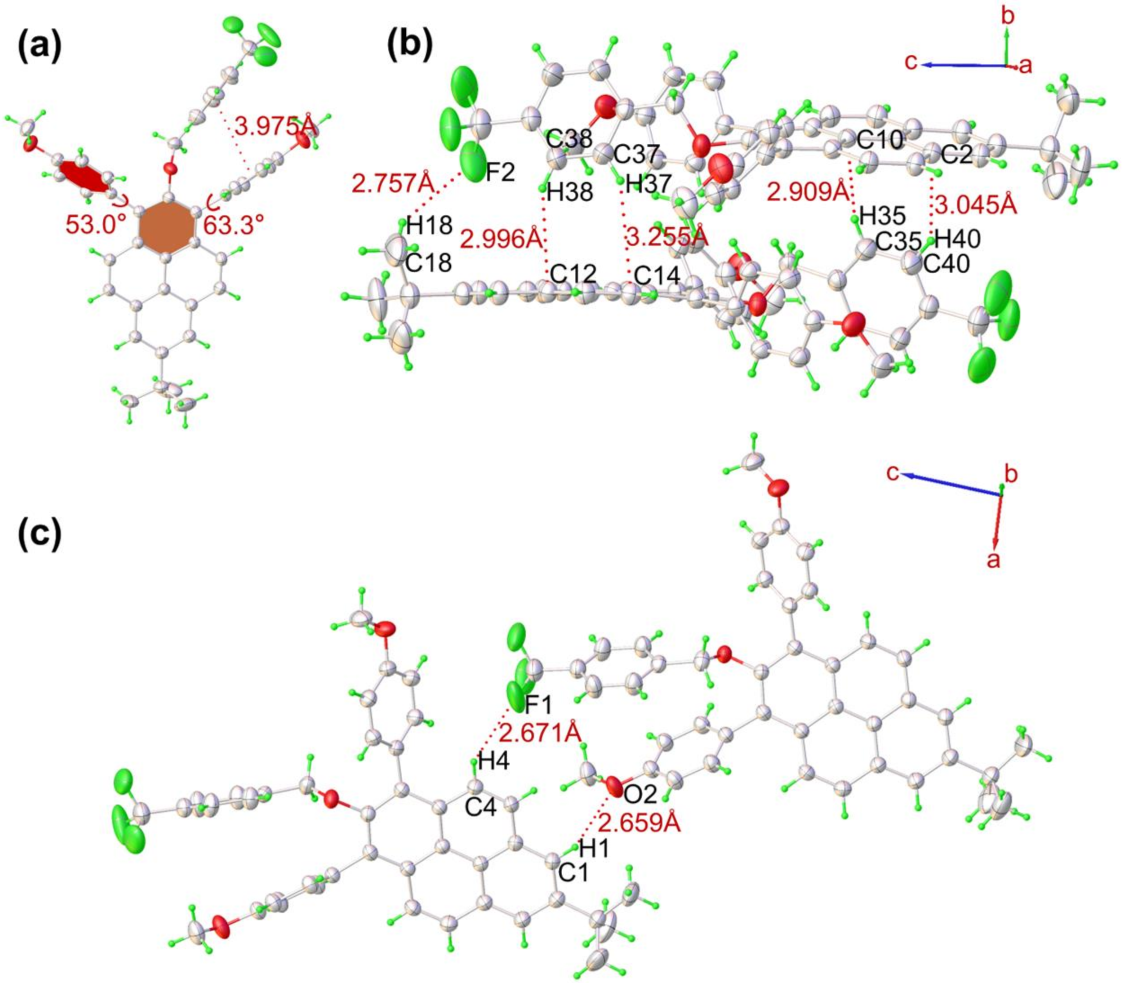

Figure 2. (a)The ORTEP view of the crystal structure **3a** with 50% thermal ellipsoids, and the packing structures formed by weak intra/intermolecular interactions (b) along the *b*-axis and (c) along the *c*-axis.

3.4 Photophysical Properties

The photophysical properties of compounds **2** and **3** were carefully examined and the detailed results are summarized in Table 1. As presented in Figure 3A, the dilute THF solution of compound **2** (~10^{-5} M) exhibited a very similar absorption performance to the corresponding compound **3**, respectively, indicated that the 4-(trifluoromethyl) benzyl moiety exerted a limited effect on the absorption band. This is ascribed to the node plane at the 2-position, resulting in weak electronic communication between the substituent group and the pyrene core.[47] Compounds **2a** and **3a** presented almost identical and well-resolved absorption bands in the range 310-400 nm with the maximum absorption wavelength ($\lambda_{\text{max, abs}}$) at 356 nm. While compounds **2b** and **3b**, **2c** and **3c** exhibited broad π-π* absorption bands at 325-400 nm and 300-400 nm, respectively, rooted in the extended conjugated structures of the pyrene chromophores with the TPA or TPE segments at the 1,3-positions. THF solutions of the luminogens **2c** and **3c** both exhibited $\lambda_{\text{max, abs}}$ at 354 nm, while the $\lambda_{\text{max, abs}}$ of **2b** and **3b** in THF solution was red-shifted to 365 nm and 368 nm, respectively, which resulted from the better electron-donor ability of the TPA group relative to the TPE unit. It is worth noting that the molar extinction coefficient (ε) of **3b** and **3c** exhibited a significant enhancement compared with **2b** and **2c**, which was assigned to intramolecular interactions such as C–H…π and/or π-π interactions between the 4-(trifluoromethyl) benzyl segment and the neighboring phenyl group in the TPA and TPE units leading to an extension of the π-conjugation.[48] Upon irradiation, the compounds **2** emitted deep-blue fluorescence in THF solution with the maximum emission peaks located in the range from 408 nm to 459 nm (Figure 3B). The compound **2b** exhibited a large, red-shifted emission compared with **2a** and **2c**, which was assigned to the stronger electron-donor capacity of the TPA unit. When the hydroxyl group was modified with a 4-(trifluoromethyl) benzyl moiety, the corresponding compounds **3b** and **3c** show a red-shifted emission with the maximum emission peak located at 465 nm and 444 nm, respectively. This red shift may be attributed to the intensive intramolecular interactions (such as C-H···F interactions) and a solvent effect. On the other hand, although the emission peaks of **2** and **3** in the solid state were shifted to 427 nm (**2a**), 459 nm (**2b**), 457 nm (**2c**), 422 nm (**3a**), 451 nm (**3b**) and 436 nm (**3c**) compared with their THF solutions (Figure 3C), the compounds **3** containing 4-(trifluoromethyl) benzyl moiety displayed a remarkable 5~21 nm blue-shifted emission compared with the corresponding compounds **2** in the solid state. Similarly, 4-(trifluoromethyl) benzyl moiety also displayed similar blue-shifted emission compared with the corresponding compounds **2** as a film (Figure S31). It is reasonable to infer that the bulky 4-(trifluoromethyl) benzyl moiety at the 2-position can exert an efficient steric effect, resulting in a more rigid molecular configuration in the aggregated state, which is consistent with our previous report.[41]

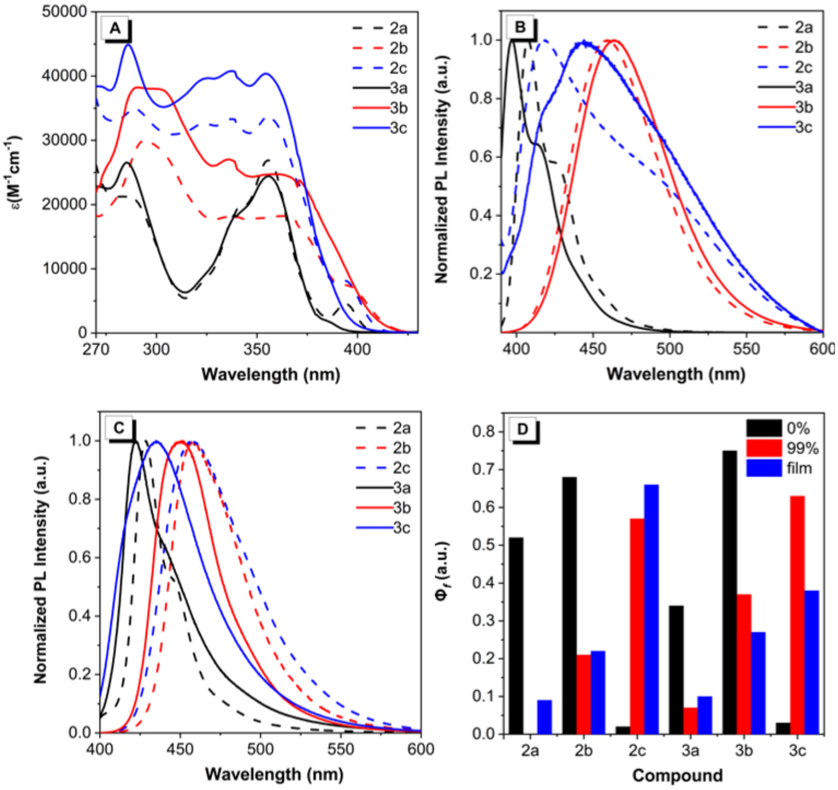

Figure 3. A): Absorption spectra and B): Emission spectra of compounds **2** and **3** in THF (10 μM); C) Emission spectra of compounds **2** and **3** in the powdered solid; D) Quantum yields of compounds **2b**-**3c** in THF/H_2O mixtures with water fractions (f_w) of 0% (black), 99% (red) and as a film (blue).

Moreover, all the compounds presented a narrow-band emission with FWHM of 28 nm, 50 nm, 61 nm, 37 nm, 45 nm and 59 nm for **2a-3c** in the solid state, respectively. The compounds **3** containing the 4-(trifluoromethyl) benzyl moiety showed a narrower FWHM compared with the corresponding hydroxyl-substituted compounds **2** except for **2a** and **3a**. Moreover, the compounds **2-3** exhibit a relatively narrower FWHM compared with previous reported systems (detailed molecular structures are summarized in Table S2). Otherwise, although the PLQY is 9% for **2a**, 22% for **2b**, 10% for **3a** and 27% for **3b** in the thin film, which is lower than in its THF solution, the 4-(trifluoromethyl) benzyl-decorated pyrene compounds **3** showed a relatively high PLQY in the solid state compared to the corresponding compounds **2**. This suggested that the effective steric hindrance of the 4-(trifluoromethyl) benzyl group can not only prevent the aggregation-quenched fluorescence behavior, but can also tune the fluorescence to the blue region, resulting in high-performance blue emission properties.

Table 1. Photophysical properties of compounds **2** and **3**.

Comd.	$\lambda_{max\ abs}$ [a] (nm)	λ_{maxPL} (nm)	τ(ns)	Φ_f	α_{AIE} [e]	$K_r(10^7 s^{-1})$ [f]	$K_{nr}(10^7 s^{-1})$ [g]	FWHM (nm)	CIE (X,Y) [h]
2a	356	408 [a]	10.66 [a]	0.52 [a]	0.18	4.87 [a]	4.51 [a]	33 [a]	0.16, 0.03
		407 [b]	2.16 [b]	-		-	-	43 [b]	
		427 [d]	18.77 [c]	0.09 [c]		0.48 [c]	4.85 [c]	28 [d]	
2b	365	459 [a]	2.90 [a]	0.68 [a]	0.32	23.4 [a]	11.08 [a]	65 [a]	0.14, 0.13
		455 [b]	1.32 [b]	0.21 [b]		15.9 [b]	59.86 [a]	55 [b]	
		459 [d]	1.94 [c]	0.22 [c]		11.3 [c]	40.24 [c]	50 [d]	
2c	354	418 [a]	1.34 [a]	0.02 [a]	33	1.49 [a]	73.14 [a]	106 [a]	0.14, 0.15
		479 [b]	2.28 [b]	0.57 [b]		25.00 [b]	18.86 [b]	90 [b]	
		457 [d]	2.68 [c]	0.66 [c]		24.63 [c]	12.68 [c]	61 [d]	
3a	356	397 [a]	13.64 [a]	0.34 [a]	0.29	2.48 [a]	4.85 [a]	33 [a]	0.16, 0.06
		449 [b]	3.52 [b]	0.07 [b]		1.99 [b]	26.42 [b]	100 [b]	
		422 [d]	11.34 [c]	0.10 [c]		0.88 [c]	7.94 [c]	37 [d]	
3b	368	465 [a]	3.13 [a]	0.75 [a]	0.36	23.96 [a]	8.01 [a]	68 [a]	0.14, 0.07
		450 [b]	2.37 [b]	0.37 [b]		15.61 [b]	26.58 [b]	58 [b]	
		451 [d]	2.07 [c]	0.27 [c]		13.04 [c]	35.27 [c]	45 [d]	
3c	354	444 [a]	1.80 [a]	0.03 [a]	12.6	1.66 [a]	53.89 [a]	112 [a]	0.15, 0.07
		487 [b]	7.19 [b]	0.63 [b]		8.76 [b]	5.15 [b]	103 [b]	
		436 [d]	3.37 [c]	0.38 [c]		11.27 [c]	18.40 [c]	59 [d]	

[a] Measured in THF solutions. [b] Measured in in THF/water mixtures at different f_{w} 99%.

[c] Measured in film. [d] Measured as a powdered solid.

[e] $\alpha = \Phi_{\mathrm{film}}/\Phi_{\mathrm{soln}}$. [f] k_r = radiative decay rate (Φ/τ). [g] k_{nr} = nonradiative decay rate ($1/\tau - k_r$).

[h] CIE coordinates of compound **2**-**3** as powdered solids.

Additionally, the concentration-dependent fluorescence spectra were investigated, the results are displayed in Figure S20. Except for compounds **2b** and **3b,** the four luminogens **2a**, **3a**, **2c** and **3c** showed a relatively large concentration-dependent blue-shifted emission behavior as the concentration gradually increased, which suggested the molecular structure become more rigid with the enhanced molecular aggregation. Furthermore, the absorption and emission behavior of these compounds in different solvents of various polarity were examined (Figures S21-S26). All compounds displayed very similar absorption performances ranging from the nonpolar solvent cyclohexane (Cy) to the highly polar dimethyl sulfoxide (DMSO), with no obvious shift in absorption bands and only a slight difference in absorbance. Nevertheless, the maximum emission peaks of **2b** and **3b** were red-shifted from ~420 nm to ~510 nm with increased solvent polarity. The presence of weak donor-acceptor interactions between the TPA group and the pyrene cores in **2b** and **3b**, resulted in charge transfer processes. Given that the polar solvents can stabilize the charge-transfer complex, this led to a red-shifted wavelength on increasing the solvent polarity. On the contrary, **2c** and **3c** exhibited only a slight change for the maximum emission peaks in weakly and highly polar solvents such as 1,4-dioxane, THF, DMF, ACN and DMSO. The maximum emission peaks in the nonpolar solvent cyclohexane were red-shifted to ~500 nm, indicating the formation of excimers in this nonpolar solvent.[49,50] As for **2a** and **3a**, their emission behavior was found to be independent of the polarity of the solvents as well as the absorption performances (Table S3).

3.4 AIE characteristics

Previously, it was reported that a set of Y-shaped blue emitters 1,3-aryl-substituted pyrene,[51] and the TPA- or TPE-decorated pyrenes exhibit AIE characteristics.[52] In order to demonstrate the fluorescence performance of compounds **2** and **3** in the aggregated states, their emission spectra in THF/H_2O mixtures with various water fractions (f_w) were examined. As depicted in Figure 4, compound **2c** possessed weak blue fluorescence with the maximum emission peak located at 418 nm (in THF solution $f_w = 0$). When f_w was increased to 99%, the emission intensity was significantly enhanced and the maximum emission peak was red-shifted by ~70 nm. With the raised water fraction, molecular aggregations induced the restriction of the intramolecular rotations in the twisted molecular architectures and thus resulted in an AIE effect. Compound **3c** exhibited similar fluorescence behavior in THF/water mixture as did compound **2c**. The compound **3c** exhibited weak blue emission in THF solution with a maximum emission peak at 444 nm, and the emission intensity remains unchanged when the f_w was less than 40%. When f_w was increased to 50%, the emission intensity was rapidly enhanced by 160-fold. After continuing to increasing the f_w, the emission intensity slightly decreased with a red-shifted emission peak at 487 nm, but the emission intensity is still up to ~120-fold larger compared with that in THF solution. Thus, both compounds **2c** and **3c** are AIE active. The photoluminescence quantum yield (PLQY) of **2c** and **3c** in thin film were 66% and 38%, respectively, and were clearly enhanced by 33-fold and 13-fold *versus* that in pure THF solution, respectively, which further verified their AIE properties. In addition, the compound **3c** containing the 4-(trifluoromethyl) benzyl moiety show a relatively low PLQY, which may be ascribed to the strengthening of the intermolecular C-H···F interaction. The morphology of compounds **2b**, **2c** **3b** and **3c** were investigated by Scanning Electron Microscopy (SEM). As shown in Figures S35-S38, the compounds **2c** and **3c** exhibit relatively well-distributed nanoparticles at f_w= 99% and in the thin film state, while at f_w = 0%, the compounds self-assemble to irregular aggregates, indicating that the high-quality, well-distributed nanoparticles with a uniform arrangement mode can enhance the emission in the solid-state. As for **2b** and **3b**, the compounds form irregular patches at f_w = 0%, 99% and the thin film state. These experimental results are agreement with previous reports.[53]

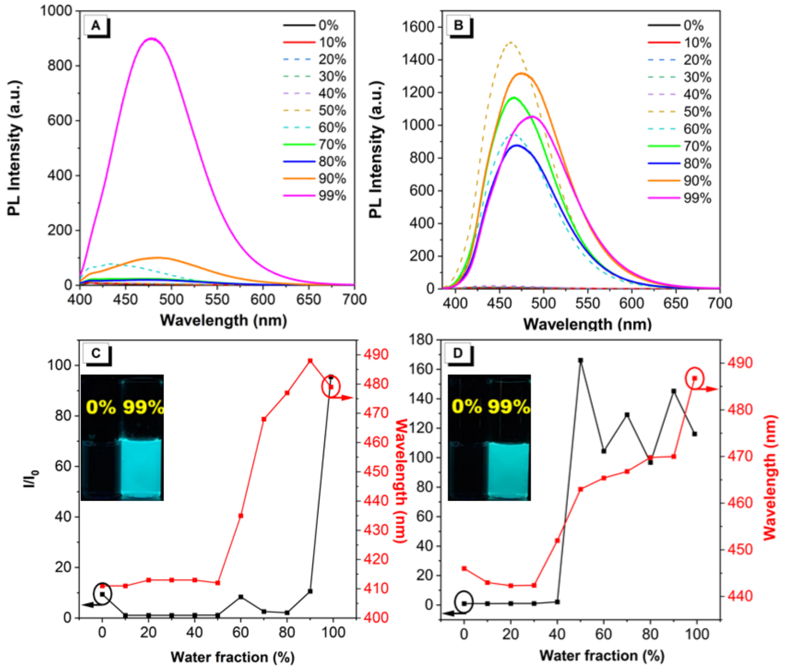

Figure 4. Emission spectra of (A) **2c** and (B) **3c** in THF/H_2O mixtures with various water fractions (f_w) (10 μM). Plot of relative PL intensity I/I_0 at different water fractions for (C) **2c** and (D) **3c**. Inset: fluorescent images of **2c** and **3c** in THF/H_2O mixtures at different f_w (0% and 99%) taken under 365 nm irradiation.

Furthermore, the transient fluorescent spectra were investigated and the corresponding decay curves of **2** and **3** in THF solution, THF/H_2O mixture with 99% water fraction and thin film are depicted in Tables S5 and 1. The fluorescence lifetimes (τ) of **2c** in solution and thin film were found to be 1.34 and 2.68 ns, respectively. On the basis of this data, the corresponding radiative decay rates (K_r) and the nonradiative decay rates (K_{nr}) were calculated according to the formulae[54]: $K_r = QY/\tau$ and $K_{nr} = 1/\tau - K_r$. The K_r of **2c** in thin film was calculated to be 24.63×10^7 S^{-1}, showing a significant promotion relative to the 1.49×10^7 S^{-1} in the solution state, while the value of K_{nr} dropped from 73.14×10^7 S^{-1} to 12.68×10^7 S^{-1}, respectively. The related values of K_r and K_{nr} for compound **3c** exhibited similar variation trends. These results again identified the higher emission efficiency for **2c** and **3c** in the aggregation state and is consistent with the above PL results. Thus, the TPE-containing luminogens **2c** and **3c** both exhibited representative AIE characteristics. However, the emission intensity of **2a, 2b, 3a** and **3b** were reduced gradually on addition of water, with a red-shifted emission (Figures S27-S30). This contributes to the excessive poor solvent maybe induced the molecular tight stacking, resulting in the enhanced intermolecular interactions and thus blocking the fluorescence output. Thus, the compounds **2a, 2b, 3a** and **3b** are non-AIE-active materials.

3.5 DFT calculations

The optimized molecular geometries and the electronic distribution of compounds **2** and **3** were investigated by density functional theory (DFT) calculations via the B3LYP/6-311G (d,p) procedure with the Gaussian 09 program. As depicted in Figure 5, the electronic distribution of the HOMO and LUMO in the compounds **2a**, **2c**, **3a**, **3c** were dominantly localized over the whole pyrene core with HOMO levels of -5.27 eV, -5.31 eV, -5.40 eV and -5.43 eV, and LUMO levels of -1.57 eV, -1.78 eV, -1.80 eV and -1.92 eV respectively. The similar energy gap between **2a** and **2c**, **3a** and **3c** suggested their close absorption wavelength, which is consistent with the spectral results. While the HOMO and LUMO energy levels of **2b** and **3b** were separated to some extent, the HOMO energy levels of **2b** and **3b** were mainly concentrated at the pyrene core, whilst the electron distribution of the LUMO in compounds **2b** and **3b** were delocalized over the whole conjugated skeleton, especially localized on the TPA moiety, which was attributed to the electron-donor ability of the TPA group. The separated HOMO and LUMO energy level led to a smaller energy gap for **2b** and **3b** with 3.37 eV and 3.26 eV respectively, resulting in red-shifted absorption wavelengths compared with the other four compounds. These results indicated that the introduction of the 4-(trifluoromethyl) benzyl exerted no obvious influence on the electron cloud distribution, while the electronic effect of the conjugated groups directly connected to the pyrene core had a great influence on the electron cloud distribution of the whole molecule.

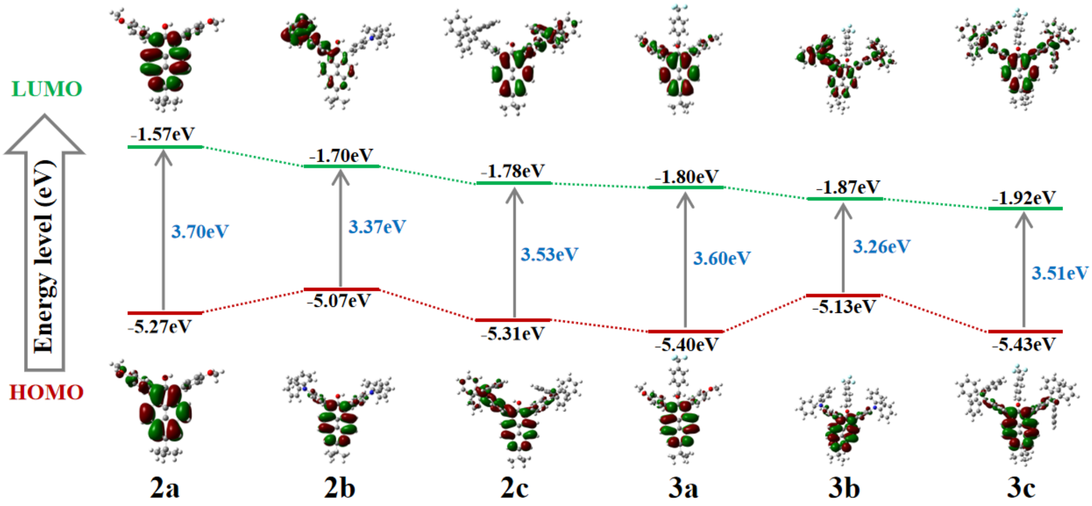

Figure 5. Computed molecular orbital plots (B3LYP/6-31G*) of **2** and **3**.

4. Conclusions

In this contribution, a series of new *Y*-shaped luminogens **2** and **3** were successfully prepared from a pyrene-based intermediate 2-hydroxyl-7-*tert*-butyl-1,3-bromopyrene (1), prepared by our research group. Three-dimensional TPA and TPE moieties were introduced at the 1,3-positions, and a bulky benzyl group was attached at the 2-position, respectively. As expected, the thermal stability and the optical properties of the *Y*-shaped pyrene-based emitters could be readily tuned by molecular engineering. (1) The compounds **2** showed great thermal stability with higher T_d compared with compounds **3** containing benzyl units, (2) the compounds **2** with the hydroxy group present at the 2-position of pyrene show a low PLQY, owing to the strengthening of the intermolecular hydrogen bond interactions, (3) when the hydroxyl group was replaced by the bulky benzyl group, the compounds **3** showed a blue-shifted fluorescence with narrow-band emission in the solid state. This is because of the bulky benzyl group that not only plays a significant role to regulate the intermolecular interactions, resulting in enhanced emission in aggregated states, but also can narrow the emission band via rigidifying the molecular conformation. Thus, the systematic exploration of the photophysical properties of the pyrene-based blue emitters in this work will provide an efficient molecular strategy for developing high-performance, narrow-band pyrene-based blue emitters with great potential for application in blue OLED devices.

2. Experimental Section

2.1 Materials

Unless otherwise stated, all reagents used were purchased from commercial sources and were used without further purification. The intermediate 7-*tert*-butyl-2-hydroxyl-1,3-dibromopyrene (**1**) was synthesized from 7-*tert*-buty-2-hydroxylpyrene following our previous report.[41] The compounds **2a-3c** were synthesized by a Suzuki reaction using (**1**) as starting material, and then were involved in a Williamson reaction to afford the corresponding compounds **3a-3c** in high yields, respectively.

2.2 Characterization

^{1}H and ^{13}C{^{1}H} NMR spectra were recorded on a Bruker AV 400M spectrometer using chloroform-d solvent and tetramethylsilane as internal reference; *J*-values are given in Hz. High-resolution mass spectra (HRMS) were recorded on a LC/MS/MS, which consisted of a HPLC system (Ultimate 3000 RSLC, Thermo Scientific, USA) and a Q Exactive Orbitrap (QE orbitrap type) mass spectrometer. UV-vis absorption spectra and photoluminescence (PL) spectra were recorded on a Shimadzu UV-2600 and the Hitachi F-4700 spectrofluorometer. PL quantum yields were measured using absolute methods using a Hamamatsu C11347-11 Quantaurus-QY Analyzer. The quantum lifetimes were recorded on an Edinburgh FLS 980 instrument and measured using a time-correlated single-photon counting method. Thermogravimetric analysis was carried on a Mettler Toledo TGA/DSC3+ under dry nitrogen at a heating rate of 10 °C/min. The quantum chemistry calculation was performed on the Gaussian 09 (B3LYP/6–311G (d,p) basis set) software package.

2.3 X-ray Crystallography

Crystallographic data for the compound **3a** was collected on a Bruker APEX 2 CCD diffractometer with graphite monochromated Mo Kα radiation (λ = 0.71073 Å) in the ω scan mode.[55,56] The structure was solved by charge flipping or direct methods algorithms and refined by full-matrix least-squares methods on F^2.[57] All esds (except the esd in the dihedral angle between two l.s. planes) were estimated using the full covariance matrix. The cell esds were considered individually in the estimation of esds in distances, angles and torsion angles. Correlations between esds in cell parameters were only used when they were defined by crystal symmetry. An approximate (isotropic) treatment of cell esds was used for estimating esds involving l.s. planes. The final cell constants were determined through global refinement of the xyz centroids of the reflections harvested from the entire data set. Structure solution and refinements were carried out using the SHELXTL-PLUS software package.[57] Data (excluding structure factors) on the structures reported here have been deposited with the Cambridge Crystallographic Data Centre. CCDC 2315003 (**3a**) contains the supplementary crystallographic data for this paper. These data could be obtained free of charge from The Cambridge Crystallographic Data Centre via www.ccdc.cam.ac.uk/data_request/cif.

2.4 Synthetic procedures

Synthesis of 7-tert-butyl-2-hydroxyl-1,3-dibromopyrene (1): Under a nitrogen atmosphere, 7-*tert*-butyl-2-hydroxylpyrene (1.64 g, 6.0 mmol, 1.0 eq.) and *N*-bromosuccinimide (NBS) (3.3 g, 18.6 mmol, 3.1 eq.) were added into a round-bottom flask containing dry DCM (30 mL), and the mixture was stirred at room temperature for 18 h. After the reaction, the mixed solution was quenched by H_2O and extracted by DCM (3 × 50 mL) three times, and the combined organic layer was washed with water and brine. The combined organic layer was dried with anhydrous $MgSO_4$ and then evaporated. The crude product was further purified by silica gel column chromatography using *n*-hexane/dichloromethane ($V_{\text{n-hexane}}$:$V_{\text{dichloromethane}}$=4:1) as eluent to obtain a gray solid powder 7-*tert*-butyl-2-hydroxyl-1,3-dibromopyrene **(1)** (1.47 g, 57%). ^{1}H NMR (400 MHz, DMSO-d_6) δ 10.44 (s, 1H), 8.44 (s, 2H), 8.35 (d, *J* = 9.3 Hz, 2H), 8.31 (d, *J* = 9.2 Hz, 2H), 1.54 (s, 9H) ppm; the result is consistent with our previous report.

Compounds **2a**, **2b** and **2c** were synthesized by the same procedure but by varying the corresponding arylboronic acid ester. The detailed synthetic procedure of **2a** is illustrated below as an example.

Synthesis of 7-tert-butyl-2-hydroxyl-1,3-bis(4-methoxyphenyl)phenyl)pyrene (2a): Under a nitrogen atmosphere, 7-*tert*-butyl-2-hydroxyl-1,3-dibromopyrene **(1)** (429 mg, 1.0 mmol, 1.0 eq.), 2-(4-methoxyphenyl)-4,4,5,5-tetramethyl-1,3,2-dioxaborolane (468 mg, 2.0 mmol, 2.0 eq.) and K_2CO_3 (690 mg, 5 mmol, 5.0 eq.) were added into a round bottomed flask containing a mixture solution of toluene, ethanol and water (12 mL) ($V_{toluene}$:$V_{ethanol}$:V_{water} = 4:1:1). The mixture was stirred for 5 min and then $Pd(PPh_3)_4$ (100 mg, 0.08 mmol) was added, The mixture was stirred at 90 °C (oil bath) for 24 h. After cooling, the mixed solution was quenched by H_2O and extracted by DCM (3 × 50 mL) three times, and the organic layer was washed with water and brine. The combined organic layer was dried with anhydrous $MgSO_4$ and then evaporated. The crude product was further purified by silica gel column chromatography using *n*-hexane/dichloromethane ($V_{n\text{-hexane}}$:$V_{dichloromethane}$=2:1) as eluent to obtain a light yellow solid powder 7-*tert*-butyl-2-hydroxyl-1,3-bis(4-methoxyphenyl)phenyl)pyrene **(2a)** (374 mg, 77%, melting point: 276 °C). ^{1}H NMR (400 MHz, $CDCl_3$) δ 8.17 (s, 2H), 7.96 (d, *J* = 9.2 Hz, 2H), 7.79 (d, *J* = 9.2 Hz, 2H), 7.52 (d, *J* = 8.5 Hz, 4H), 7.15 (d, *J* = 8.6 Hz, 4H), 5.44 (s, 1H), 3.93 (s, 6H), 1.58 (s, 9H) ppm. $^{13}C\{^1H\}$ NMR (100 MHz, $CDCl_3$) δ 159.4, 148.3, 148.1, 132.6, 130.1, 130.0, 128.0, 127.5, 124.8, 123.1, 122.5, 120.0, 114.5, 77.4, 77.1, 76.7, 55.4, 35.1, 31.9 ppm. HRMS (FTMS + p APCI) m/z: $[M+H]^+$ Calcd for $C_{34}H_{30}O_3$ 487.2195; Found, 487.2266.

Synthesis of 7-tert-butyl-2-hydroxyl-1,3-bis(4-(diphenylamino)phenyl)pyrene (2b): light yellow solid powder, 72% yield, melting point>300 °C. ^{1}H NMR (400 MHz, $CDCl_3$) δ 8.17 (s, 2H), 7.98 (d, *J* = 9.3 Hz, 2H), 7.89 (d, *J* = 9.2 Hz, 2H), 7.44 (d, *J* = 8.5 Hz, 4H), 7.31 (q, *J* = 8.7 Hz, 12H), 7.27-7.20 (m, 8H), 7.08 (t, *J* = 7.2 Hz, 4H), 5.58 (s, 1H), 1.58 (s, 9H) ppm. $^{13}C\{^1H\}$ NMR (100 MHz, $CDCl_3$) δ 148.1, 147.6, 132.2, 130.1, 130.0, 129.4, 128.8, 128.0, 124.8, 123.3, 123.3, 123.2, 122.5, 53.4, 35.1, 31.9 ppm. HRMS (FTMS + p APCI) m/z: $[M+H]^+$ Calcd for $C_{56}H_{44}N_2O$ 761.3454; Found, 761.3499.

Synthesis of 7-tert-butyl-2-hydroxyl-1,3-bis(4-(1,2,2-triphenylvinyl)phenyl)pyrene (2c): white solid powder, 77% yield, melting point>300 °C. ^{1}H NMR (400 MHz, $CDCl_3$) δ 8.24 (s, 2H), 8.02 (d, *J* = 9.2 Hz, 2H), 7.73 (d, *J* = 9.2 Hz, 2H), 7.41-7.32 (m, 10H), 7.28 (d, *J* = 7.2 Hz, 10H), 7.25–7.16 (m, 18H), 5.40 (s, 1H), 1.65 (s, 9H) ppm. $^{13}C\{^1H\}$ NMR (100 MHz, $CDCl_3$) δ 162.6, 148.2, 147.5, 143.8, 143.6, 143.5, 143.4, 141.7, 140.7, 133.5, 131.9, 131.5, 131.4, 131.3, 130.7, 130.0, 129.9, 128.0, 127.8, 127.7, 126.7, 126.6, 126.6, 124.7, 123.2, 122.9, 122.5, 119.9, 41.0, 36.5, 35.1, 31.9, 31.4 ppm. HRMS (FTMS + p APCI) m/z: $[M+H]^+$ Calcd for $C_{72}H_{54}O$ 935.4175; Found, 935.4231.

Compounds **3a**, **3b** and **3c** were synthesized by the same procedure but by varying the corresponding compounds **2**. The detailed synthetic procedure of **3a** is illustrated below as an example.

Synthesis of 7-tert-butyl-2-((4-(trifluoromethyl)benzyl)oxy)-1,3-bis(4-methoxyphenyl) pyrene (3a)**:** Under a nitrogen atmosphere, 7-*tert*-butyl-2-hydroxyl-1,3-bis(4-methoxyphenyl)pyrene **(2a)** (308 mg, 0.63 mmol, 1.0 eq.), 1-(bromomethyl)-4-(trifluoromethyl)benzene (608 mg, 2.55 mmol, 4.0 eq.) and Cs_2CO_3 (1.24 g, 3.8 mmol, 6.0 eq.) were added into a round-bottom flask containing dry DMF (20 mL). The mixture was stirred at 130 °C (oil bath) for 24 h. After cooling, the mixture was quenched by water and extracted three times with DCM (3×50 mL), the organic layer was successively washed by water and brine, and the combined organic extracts were dried with anhydrous magnesium sulfate ($MgSO_4$), and finally evaporated. The crude product was further purified by silica gel column chromatography using *n*-hexane/dichloromethane ($V_{n\text{-hexane}}$:$V_{\text{dichloromethane}}$=3:1) as eluent to obtain a light white solid powder 7-*tert*-butyl-2-((4-(trifluoromethyl)benzyl)oxy)-1,3-bis(4-methoxyphenyl)pyrene **(3a)** (325 mg, 80%, melting point: 255 °C). ^1H NMR (400 MHz, $CDCl_3$) δ 8.19 (s, 2H), 7.98 (d, *J* = 9.3 Hz, 2H), 7.92 (d, *J* = 9.2 Hz, 2H), 7.53 (d, *J* = 8.7 Hz, 4H), 7.36 (d, *J* = 7.9 Hz, 2H), 7.09 (d, *J* = 8.6 Hz, 4H), 6.65 (d, *J* = 7.9 Hz, 2H), 4.30 (s, 2H), 3.94 (s, 6H), 1.58 (s, 9H) ppm. $^{13}C\{^1H\}$ NMR (100 MHz, $CDCl_3$) δ 159.1, 148.9, 140.8, 132.6, 130.9, 130.7, 130.3, 128.9, 128.6, 127.9, 125.2, 124.9, 122.5, 113.7, 74.3, 55.5, 35.2, 31.9, 29.7 ppm. HRMS (FTMS + p APCI) m/z: $[M+H]^+$ Calcd for $C_{42}H_{35}F_3O_3$ 645.2538; Found, 645.2604.

Synthesis of 4,4'-(7-tert-butyl-2-((4-(trifluoromethyl)benzyl)oxy)pyrene-1,3-diyl)bis(N,N-diphenylaniline) (3b)**:** light yellow solid powder, 63% yield, melting point>300 °C. ^1H NMR (400 MHz, $CDCl_3$) δ 8.21 (s, 2H), 8.03 (s, 4H), 7.53 (t, *J* = 8.4 Hz, 6H), 7.30 (dd, *J* = 7.9, 4.3 Hz, 12H), 7.22 (d, *J* = 7.4 Hz, 8H), 7.10 – 7.05 (m, 4H), 6.96 (d, *J* = 7.9 Hz, 2H), 4.41 (s, 2H), 1.59 (s, 9H) ppm. $^{13}C\{^1H\}$ NMR (100 MHz, $CDCl_3$) δ 147.8, 147.1, 132.4, 131.0, 130.7, 130.6, 130.2, 129.4, 128.6, 128.0, 125.2, 124.4, 123.5, 123.1, 122.6, 31.9 ppm. HRMS (FTMS + p APCI) m/z: $[M+H]^+$ Calcd for $C_{64}H_{49}F_3N_2O$ 919.3797; Found, 919.3839.

Synthesis of 7-tert-butyl-2-((4-(trifluoromethyl)benzyl)oxy)-1,3-bis(4-(1,2,2-

triphenylvinyl)phenyl)pyrene (3c): white solid powder, 49% yield, melting point>300 °C. ^{1}H NMR (400 MHz, $CDCl_3$) δ 8.20 (s, 2H), 7.98 (d, J = 9.3 Hz, 2H), 7.74 (d, J = 9.2 Hz, 2H), 7.48 (d, J = 8.0 Hz, 2H), 7.35 (d, J = 8.1 Hz, 4H), 7.28 – 7.21 (m, 7H), 7.18 – 7.05 (m, 29H), 6.84 (d, J = 7.9 Hz, 2H), 1.59 (s, 9H) ppm. $^{13}C\{^1H\}$ NMR (100 MHz, $CDCl_3$) δ 149.0, 143.8, 143.6, 143.1, 141.5, 140.8, 134.7, 131.5, 131.4, 131.3, 131.1, 131.0, 130.8, 130.6, 130.2, 128.3, 127.9, 127.8, 127.7, 127.6, 126.6, 126.6, 125.0, 122.6 ppm. HRMS (FTMS + p APCI) m/z: $[M+H]^+$ Calcd for $C_{80}H_{59}F_3O$ 1093.4518; Found, 1093.4572.

ASSOCIATED CONTENT

Data Availability Statement

The data underlying this study are available in the published article and its Supporting Information.

Supporting Information

The Supporting Information is available free of charge on the ACS Publications website.

Additional experimental methods of compounds **1**, **2** and **3**. Detailed experimental characterization data, including NMR spectra, HRMS, absorption and fluorescence spectra.

AUTHOR INFORMATION

Corresponding Author

Xiang Su - Guangdong University of Technology, Guangzhou 510006, P. R. China, orcid.org/0000-0002-6346-7666; E-mail: suxiang2022@gdut.edu.cn.

Xing Feng - Guangdong University of Technology, Guangzhou 510006, P. R. China, orcid.org/0000-0002-4273-979X; E-mail: hyxhn@sina.com.

Authors

Zhixin Xie – Guangdong University of Technology, Guangzhou 510006, P. R. China.

Wei Liu - Guangdong University of Technology, Guangzhou 510006, P. R. China.

Yiwei Liu - Guangdong University of Technology, Guangzhou 510006, P. R. China.

Xinyi Song - Guangdong University of Technology, Guangzhou 510006, P. R. China.

Heng Zheng - Guangdong University of Technology, Guangzhou 510006, P. R. China.

Carl Redshaw - Chemistry, School of Natural Sciences, University of Hull, Hull, Yorkshire HU6 7RX, UK.

Author Contributions

Zhixin Xie: Investigation, resources and visualization. Wei Liu: Investigation. Xinyi Song: Investigation. Heng Zheng: Investigation. Xiang Su: Data curation, conceptualization and Writing - review & editing. Carl Redshaw: Writing - review & editing. Xing Feng: Data curation, conceptualization, Writing-original draft, supervision, project administration.

Notes

The authors declare no competing financial interest.

ACKNOWLEDGMENT

This work was supported by the National Natural Science Foundation of China (21975054), Guangzhou Basic and Applied Basic Research Foundation (2023A04J1372), the Open Fund of Guangdong Provincial Key Laboratory of Luminescence from Molecular Aggregates, Guangzhou 510640, China (South China University of Technology) (2019B03 0301003), Science and Technology Planning Project of Hunan Province (2018TP1017), CR thanks the University of Hull for support. The authors thank Prof. Qilong Zhang (Guizhou Medical University) for refining the crystal structure.

REFERENCES

(1) D Singh, V.; Gupta, N.; Gesiorski, J. L.; Weerasooriya, R. B.; Glusac, K. D. Photophysics of nanographenes: from polycyclic aromatic hydrocarbons to graphene nanoribbons. *Photosyn. Res*. **2022**, *151*, 163-184.

(2) Kumar, S.; Tao, Y. T. Coronenes, Benzocoronenes and Beyond: Modern Aspects of Their Syntheses, Properties, and Applications. *Chem. Asian. J.* **2021**, *16*, 621-647.

(3) Wang, Z.; Peng, Q.; Huang, X.; Ma, Q.; Shao, J.; Shen, Q. Recent progress of Acenaphthylene-imide-fused polycyclic aromatic hydrocarbons: Synthesis and application. *Dyes Pigm*. **2020**, *PartA*, 108877.

(4) Bhosale, S. V.; Al Kobaisi, M.; Jadhav, R. W.; Morajkar, P. P.; Jones, L. A.; George, S. Naphthalene diimides: perspectives and promise. *Chem. Soc. Rev.* **2021**, *50*, 9845-9998.

(5) Oyamada, T.; Uchiuzou, H.; Akiyama, S.; Oku, Y.; Shimoji, N.; Matsushige, K.; Sasabe, H.; Adachi, C. Lateral organic light-emitting diode with field-effect transistor characteristics. *J. Appl. Phys.* **2005**, *98*, 074506.

(6) Hwang, J.; Nagaraju, P.; Cho, M. J.; Choi, D. H. Aggregation-induced emission luminogens for organic light-emitting diodes with a single-component emitting layer. *Aggregate.* **2022**, e199.

(7) Huangfen, L.; Jinglong, C.; Lifei, Y.; Jiamin, C.; Manjun, X.; Wenliu, Z.; Jiahui, L.; Ru, X.; Junting, Y.; Zilong, T. Easily synthesized pyrene-based nonfullerene acceptors for efficient organic solar cells. *Synth Met.* **2021**, *281*, 116904.

(8) Liu, Q.; Deng, J.; Yan, D.; Huang, X.; Liao, Y.; Tao, Q. Improving photovoltaic performance of benzothiadiazole-based small molecules: A synergistic effect of non-covalent interaction and aryl terminal group. *J. Mater. Res.* **2020**, *35*, 2967-2975.

(9) Giancane, G.; Bettini, S.; Valli, L.; Bracamonte, V.; Carraro, M.; Bonchio, M.; Prato, M. Supramolecular organic–inorganic domains integrating fullerene-based acceptors with polyoxometalate-bis-pyrene tweezers for organic photovoltaic applications. *J. Mater. Chem. C.* **2021**, *9*, 16290-16297.

(10) Vishrutha, K. S.; Hidayath, U.; Raveendra Kiran, M.; Badekai Ramachandra, B.; Airody Vasudeva, A. New green emitters based on push-pull type pyrene substituted cyanopyridones: Design strategies and utilization in organic light-emitting diodes *Dyes Pigm.* **2023**. *219, 111560.*

(11) Cheng, Z.; Du, C.; Ge, S.; Wang, Y.; Liu, F.; Chang, Y.; Lv, Y.; Lu, P. Highly efficient non-doped deep-blue organic light-emitting diodes based on pyreneimidazole derivative with external quantum efficiency > 11% and negligible efficiency roll-off. *Chem. Eng. J.* **2023**, *47*, 145867.

(12) He, J.; Hanlin, L.; Jibiao, J.; Govardhana Babu, B.; Peng, T.; Dongge, M.; Wai-Yeung, W. Orthogonal anthracene and pyrene derivatives for efficient pure deep-blue organic light-emitting diodes. *J. Mater. Chem. C.* **2023**, *11*, 6438-6443.

(13) Feng, X.; Qi, C.; Feng, H.-T.; Zhao, Z.; Sung, H. H. Y.; Williams, I. D.; Kwok, R. T. K.; Lam, Jacky, W. Y.; Qin, A.; Tang, B. Z. Dual fluorescence of tetraphenylethylene-substituted pyrenes with aggregation-induced emission characteristics for white-light emission. *Chem. Sci*. **2018**, *9*, 5679-5687.

(14) Dash, P. P.; Mohanty, P.; Behera, S.; Behura, R.; Palai, B. B.; Nath, B.; Sahoo, S. K.; Jali, B. R. Pyrene-based fluorescent chemosensor for rapid detection of water and its applications. *Methods.* **2023**, *219*, 127-138.

(15) Yu, w.; Li, S.; Ni, S.; Liu, G. Z. Advances in FRET-based biosensors from donor-acceptor design to applications. *Aggregate*. 2023, e460.

(16) Shellaiah, M.; Sun, K.-W. Pyrene-Based AIE Active Materials for Bioimaging and Theranostics Applications. *Biosensors.* **2022**, *12*, 550.

(17) Feng, X.; Wang, X.; Redshaw, C.; Tang, B. Z. Aggregation behaviour of pyrene-based luminescent materials, from molecular design and optical properties to application. *Chem. Soc. Rev*., **2023**, *52*, 6715-6753.

(18) Figueira-Duarte, T. M.; Müllen, K. Pyrene-Based Materials for Organic Electronics. *Chem. Rev*. **2011**, *111*, 7260.

(19) Borges, I.; Guimarães, R. M. P. O.; Monteiro-de-Castro, G.; Rosa, N. M. P.; Nieman, R.; Lischka, H.; Aquino, A. J. A. A comprehensive analysis of charge transfer effects on donor-pyrene (bridge)-acceptor systems using different substituents. *J Comput Chem.* **2023**, *44*, 2424-2436.

(20) Wu, Z.-H.; Huang, Z.-T.; Guo, R.-X.; Sun, C.-L.; Chen, L.-C.; Sun, B.; Shi, Z.-F.; Shao, X.; Li, H.; Zhang, H.-L. 4,5,9,10-Pyrene Diimides: A Family of Aromatic Diimides Exhibiting High Electron Mobility and Two-Photon Excited Emission. *Angew. Chem. Int. Ed.* **2017**, *56*, 13031-13035.

(21) Ma, X.; Sun, R.; Cheng, J.; Liu, J.; Gou, F.; Xiang, H.; Zhou, X. Fluorescence Aggregation-Caused Quenching versus Aggregation-Induced Emission: A Visual Teaching Technology for Undergraduate Chemistry Students. *J. Chem. Educ.* **2016**, *93*, 345-350.

(22) Islam, M. M.; Hu, Z.; Wang, Q.; Redshaw, C.; Feng, X. Pyrene-based aggregation-

induced emission luminogens and their applications. *Mater. Chem. Front*. **2019**, *3*, 762-781.

(23) Zhao, G.; Zhou, R.; Zhang, G.; Chen, H.; Ma, D.; Tian, W.; Jiang, W.; Sun, Y. A periphery hindered strategy with a dopant and sensitizer for solution-processed red TSF-OLEDs with high color purity. *J. Mater. Chem. C*. **2022**, *10*, 5230-5239.

(24) Wang, Y.; Duan, Y.; Guo, R.; Ye, S.; Di, K.; Zhang, W.; Zhuang, S.; Wang, L.A periphery cladding strategy to improve the performance of narrowband emitters, achieving deep-blue OLEDs with $\mathrm{CIE}_y < 0.08$ and external quantum efficiency approaching 20%. *Org. Electron.* **2021**, *97*, 106275.

(25) Feng, X.; Iwanaga, F.; Hu, J.-Y.; Tomiyasu, H.; Nakano, M.; Redshaw, C.; Elsegood, M. R. J.; Yamato, T. An efficient approach to the synthesis of novel pyrene-fused azaacenes. *Org. Lett.* **2013**, *15*, 3594-3597.

(26) Qu, R.; Zhen, X.; Jiang, X. Emerging Designs of Aggregation-Induced Emission Agents for Enhanced Phototherapy Applications. *CCS Chem*. **2022**, *4*, 401-419.

(27) Borjihan, Q.; Wu, H.; Dong, A.; Gao, H.; Yang, Y.-W. AIEgens for Bacterial Imaging and Ablation. *Adv. Healthc. Mater.* **2021**, *10*, 2100877.

(28) Qu, J.; Zhao, X.; Liang, Y.; Zhang, T.; Ma, P. X.; Guo, B. Antibacterial adhesive injectable hydrogels with rapid self-healing, extensibility and compressibility as wound dressing for joints skin wound healing. *Biomaterials.* **2018**, *183*, 185-199.

(29) Lou, X. Y.; Yang, Y. W. Aggregation-induced emission systems involving supramolecular assembly. *Aggregate.* **2020**, *1*, 19-30.

(30) Leung, N. L. C.; Xie, N.; Yuan, W.; Liu, Y.; Wu, Q.; Peng, Q.; Miao, Q.; Lam, J. W. Y.;

Tang, B. Z. Restriction of Intramolecular Motions: The General Mechanism behind Aggregation-Induced Emission. *Chem. Eur. J.* **2014**, *20*, 15349-15353.

(31) Chen, Y.; Lam, J. W. Y.; Kwok, R. T. K.; Liu, B.; Tang, B. Z. Aggregation-induced emission: fundamental understanding and future developments. *Mater. Horiz*. **2019**, *6*, 428-433.

(32) Domínguez, R.; Navarro, A.; García-Martínez, J. C. Styrylbenzene organogels and how the cyano groups tune the aggregation-induced emission. *Dyes Pigm*. **2021**, *29*, 109427.

(33) Zhang, X.; Wang, K.; Liu, M.; Zhang, X.; Tao, L.; Chen, Y.; Wei, Y. Polymeric AIE-based nanoprobes for biomedical applications: recent advances and perspectives. *Nanoscale.* **2015**, *7*, 11486-11508.

(34) Cai, X.; Su, S.-J. Marching Toward Highly Efficient, Pure-Blue, and Stable Thermally Activated Delayed Fluorescent Organic Light-Emitting Diodes. *Adv. Funct. Mater.* **2018**, *28*, 1802558.

(35) Feng, X.; Hu, J.-Y.; Redshaw, C.; Yamato, T. Functionalization of Pyrene To Prepare Luminescent Materials-Typical Examples of Synthetic Methodology. *Chem. Eur. J.* **2016**, *22*, 11898-11916.

(36) Yu, Z.-D.; Cao, J.-Y.; Li, H.-L.; Yang, G.; Xue, Z.-M.; Jiang, L.; Yu, J.-Y.; Wang, C.-Z.; Liu, X.-Y.; Redshaw, C.; Yamato, T. Structure-controlled intramolecular charge transfer in asymmetric pyrene-based luminogens: synthesis, characterization and optical properties. *New. J. Chem*. **2022**, *46*, 16394-16400.

(37) Zych, D.; Slodek, A. Pyrene derivatives with two types of substituents at positions 1, 3, 6, and 8 - fad or necessity. *RSC. Adv.* **2019**, *9*, 24015-24024.

(38) Wu, Z.-H.; Huang, Z.-T.; Guo, R.-X.; Sun, C.-L.; Chen, L.-C.; Sun, B.; Shi, Z.-F.; Shao, X.; Li, H.; Zhang, H.-L. 4,5,9,10-Pyrene Diimides: A Family of Aromatic Diimides Exhibiting High Electron Mobility and Two-Photon Excited Emission. *Angew. Chem. Int. Ed.* **2017**, *56*, 13031-13035.

(39) More, S.; Bhosale, R.; Choudhary, S.; Mateo-Alonso, A. Versatile 2,7-Substituted Pyrene Synthons for the Synthesis of Pyrene-Fused Azaacenes. *Org. Lett.*, **2012**, *14*, 4170-4173.

(40) Magano, J.; Dunetz, J. R. Large-Scale Applications of Transition Metal-Catalyzed Couplings for the Synthesis of Pharmaceuticals. *Chem. Rev.* **2011**, *111*, 2177-2250.

(41) Wang, X.; Zhang, J.; Mao, X.; Liu, Y.; Li, R.; Bai, J.; Zhang, J.; Redshaw, C.; Feng, X.; Tang, B. Z. Intermolecular Hydrogen-Bond-Assisted Solid-State Dual-Emission Molecules with Mechanical Force-Induced Enhanced Emission. *J. Org. Chem.* **2022**, *87*, 8503-8514.

(42) Feng, X.; Hu, J.-Y.; Iwanaga, F.; Seto, N.; Redshaw, C.; Elsegood, M. R. J.; Yamato, T. Organic Letters. Blue-Emitting Butterfly-Shaped 1,3,5,9-Tetraarylpyrenes: Synthesis, Crystal Structures, and Photophysical Properties. *Org. Lett*. **2013**, *15*, 1318-1321.

(43) Mohamed Gamal, M.; Maha Mohamed, S.; Tharwat H., M.; Santosh, U. S.; Ming-Shiuan, T.; Jung-Hui, C.; Jyh-Tsung, L.; Shiao-Wei, K. Dispersions of 1,3,4-Oxadiazole-Linked Conjugated Microporous Polymers with Carbon Nanotubes as a High-Performance Electrode for Supercapacitors. *ACS Appl. Energy Mater.* **2022**, *5*, 3677-3688.

(44) Wang, Z.-Y.; Liu, B.; Zhao, J.-W.; Ruan, G.-L.; Tao, S.-L.; Tong, Q.-X. Bipolar deep-blue phenanthroimidazole derivatives: Structure, photophysical and electroluminescent properties. *Org. Electron.* **2018**, *52*, 89-97.

(45) Zhang, L.; Zhao, H.; Hu, M.; Wang, X.; Hu, L.; Mao, H.; Yuan, Z.; Ma, W.; Chen, Y. Enhanced Efficiency and Excellent Thermostability in Organic Photovoltaics via Ternary Strategy with Twisted Conjugated Compound. *Small*. **2021**.*17*, 2103537.

(46) Deng, Y.; Yuan, W.; Jia, Z.; Liu, G. H- and J-Aggregation of Fluorene-Based Chromophores. *J. Phys. Chem. B.* **2014**, *118*, 14536–14545.

(47) Crawford, A. G.; Dwyer, A. D.; Liu, Z.; Steffen, A.; Beeby, A.; Pålsson, L.-O.; Tozer, D. J.; Marder, T. B. Experimental and Theoretical Studies of the Photophysical Properties of 2- and 2,7-Functionalized Pyrene Derivatives. *J. Am. Chem. Soc.* **2011**, *133*, 13349-13362.

(48) Monika, L.; Marilyn Daisy, M. Novel Y-shaped multi-stimuli responsive pyrene substituted quinoxaline and pyridopyrazine-based push-pull molecules showing solvatochromism, aggregation induced excimer emission, acidofluorochromism and moisture detection. *Dyes Pigm.* **2023**, *213*, 111182.

(49) Keller, S. N.; Veltri, N. L.; Sutherland, T. C. Tuning Light Absorption in Pyrene: Synthesis and Substitution Effects of Regioisomeric DonorAcceptor Chromophores. *Org. Lett*. **2013**, *15*, 4798-4801.

(50) Hogan, D. T.; Gelfand, B. S.; Spasyuk, D. M.; Sutherland, T. C. Subtle substitution controls the rainbow chromatic behaviour of multi-stimuli responsive core-expanded pyrenes. *Mater. Chem. Front*. **2020**, *4*, 268-276.

(51) Feng, X.; Hu, J.-Y.; Yi, L.; Seto, N.; Tao, Z.; Redshaw, C.; Elsegood, M. R. J.; Yamato, T. Pyrene-Based Y-shaped Solid-State Blue Emitters: Synthesis, Characterization, and Photoluminescence. *CHEM-ASIAN J.* **2012**, *7*, 2854-2863.

(52) Zeng, J.; Qiu, N.; Zhang, J.; Wang, X.; Redshaw, C.; Feng, X.; Lam, J. W. Y.; Zhao, Z.;

Tang, B. Z. Y-Shaped Pyrene-Based Aggregation-Induced Emission Blue Emitters for High-Performance OLED Devices. *Adv. Opt. Mater*. **2022**, *10*(19), 2200917.

(53) Zheng, Z.; Li, D.; Liu, Z.; Peng, H.-Q.; Sung, H. H. Y.; Kwok, R. T. K.; Williams, I. D.; Lam, J. W. Y.; Qian, J.; Tang, B. Z. *Adv. Mater.* **2019**, 1904799.

(54) Liu Y.; Mao X.; Wang X.; Bai J.; Zhang J.; Feng X.; et al. Pyrene-based asymmetric hexaarylbenzene derivatives: Synthesis, crystal structures, and photophysical properties. *J. Lumin.* **2021**, *12*, 118653.

(55) Bruker, “APEX2, SAINT and SADABS,” Bruker AXS Inc., Madison, **2009**.

(56) Bruker SHELXTL Version 5.1. (Includes XS, XL, XP, XSHELL), Bruker AXS Inc., Madison, Wisconsin, USA, **1999**.

(57) Sheldrick, G.; Sheldrick, G. M.; Sheldrick, G. M. SHELXL-97, a program for crystal structure refinement. **1997.**